Fernández-Torrijos, M., Albrecht, K.J., Hob, C.K. (2018). Dynamic modeling of a particle/supercritical CO2 heat exchanger for transient analysis and control, *Applied Energy,* v. 226, pp. 595-606

DOI: https://doi.org/10.1016/j.apenergy.2018.06.016

Dynamic modeling of a particle/supercritical CO_2 heat exchanger for transient analysis and control

M. Fernández-Torrijos[a,*], K. J. Albrecht[b], C. K. Ho[b]

Corresponding author: Tel +34 916246032. E-mail address: ftorrijo@ing.uc3m.es

[a] Universidad Carlos III de Madrid, ISE Research Group, Thermal and Fluid Engineering Department, Avda. Universidad 30, 28911 Leganés, Madrid, Spain

[b] Sandia National Laboratories, Albuquerque, NM, USA

Abstract

A dynamic model of a moving packed-bed particle-to-sCO_2 heat exchanger and control system for concentrating solar power (CSP) applications is presented. The shell-and-plate heat-exchanger model allows for numerically investigating the transient operation and control of the heat addition to the power cycle in a particle-based CSP plant. The aim of the particle-to-sCO_2 heat exchanger is to raise the sCO_2 temperature to 700 °C at a pressure of 20 MPa. The control system adjusts both the particle and sCO_2 mass flow rates as well as an sCO_2 bypass to obtain the desired sCO_2 turbine inlet and particle outlet temperatures for a prescribed thermal duty. The control system is demonstrated for disturbances in particle and sCO_2 inlet temperatures as well as changes in thermal duty for part-load operation. A feed-forward control strategy that adjusts the sCO_2 and particle mass-flow rates as functions of measured inlet temperatures and a steady-state model solution was able to return the heat exchanger to the desired operating condition, but not without experiencing significant deviations in the sCO_2 turbine inlet and particle outlet temperature (>40 °C) during the transient. To reduce both sCO_2 and particle temperature deviations, a feedback control strategy was investigated, where sCO_2 and particle mass-flow rates based on the steady-state model solution were corrected based on measured outlet temperature deviations. The feedback control strategy maintains sCO_2 turbine inlet and particle outlet temperature to within 16 °C of the set points with a three-minute settling time for step changes in inlet conditions and thermal duty. This finding demonstrates the possibility of dynamically dispatching next-generation particle-based CSP plants driving sCO_2 power cycles.

Keywords: Heat Exchanger; Shell-and-Plate; Feed-forward control; Feedback control; Supercritical CO_2; Falling particle receiver.

1. Introduction and objectives

The integration of concentrating solar power (CSP) plants onto the electric grid allows for renewable solar energy to be dynamically dispatched. This is enabled by CSP's ability to provide low-cost, high-efficiency thermal energy storage, which essentially decouples the intermittent renewable resource from the thermal load of a power cycle to meet fluctuating

demands of the electric grid. A recent study [1] has identified dynamic dispatch as the cost-optimal operating strategy for CSP plants. The desired future CSP plant will have fast ramping and turn-down capabilities, which only increase in importance as other renewable generators (i.e., photovoltaics and wind) increase penetration. For CSP plants to meet this need, fast ramping and turn-down capabilities as well as control must be demonstrated for next-generation CSP configurations.

The particle receiver has been identified [2] as one of the three potential pathways for the next-generation CSP plants to improve solar-to-electric efficiency through coupling to a supercritical carbon dioxide (sCO_2) Brayton cycle. According to the United States Department of Energy CSP Gen 3 Roadmap [2], the particle heat exchanger is one of the technology gaps that should be addressed to demonstrate high solar-to-electric conversion efficiencies for next-generation CSP. In the present paper, the transients and off-design operation of the particle-to-sCO_2 heat exchanger are discussed and a control system is proposed. This research issue has not been investigated in the past and it is critical to gain operational understanding of this key component of particle-based CSP plants prior to on-sun testing.

2. Prior Work

Solid particle receivers have been proposed to achieve higher inlet temperatures needed for sCO_2 power cycles. In the falling particle receiver configuration, particles fall through a cavity receiver and are directly irradiated by a beam of concentrated sunlight. Direct irradiation of the heat transfer media avoids the flux limitations associated with tubular central receivers. Once heated, the particles may be stored in an insulated tank and discharged to heat the power cycle working fluid [3]. The majority of research to date has focused on the development of high-efficiency and high-temperature particle solar thermal receivers [4]. Siegel et al. [5] developed a CFD model of a falling-particle cavity receiver, which was validated against experimental measurements at power levels up to 2.5 MW_{th} at Sandia National Laboratories in Albuquerque. More recently, Ho et al. [6] presented advancements in particle receiver designs including the use of porous structures in the particle flow or particle recirculation to increase the residence time in the concentrated sunlight. Air curtains near the aperture of the receiver have also been investigated to stabilize particle flow and reduce convective heat loss by external winds. Zhang et al. [7] presented an innovative solar receiver technology in which particles move upward in tubes that constitutes the solar absorber.

Supercritical CO_2 in a closed-loop Brayton cycle offers the potential of higher cycle efficiency in comparison with superheated or supercritical steam cycles at temperatures relevant for concentrating solar power (CSP). Turchi et al. [8] studied the efficiency achieved by different sCO_2 Brayton cycle configurations, and concluded that cycle configurations such as the partial cooling cycles and recompression with main-compression intercooling together with reheat can achieve greater than 50% efficiency. However, sCO_2 Brayton cycles require higher temperature heat addition than those previously integrated with central receivers. Current central receiver technologies employ either water/steam or molten nitrate salt as the heat-transfer and/or working fluid in subcritical Rankine power cycles, with inlet temperatures lower than 600 °C.

With the advancements in high-temperature particle receiver technology approaching thermal efficiencies values of 90%, the design and analysis of a heat exchanger for extracting thermal energy from the particles and transferring it to the power-cycle working fluid is required for system realization. The design and production of particle heat exchangers for fluidized bed reactors and particle cooling for industrial applications has existed for decades. However, the unique application of a particle heat exchanger for high-temperature (≥700°C), high-pressure (≥20 MPa) sCO_2 has not been demonstrated [2]. Gomez-Garcia et al. [9] developed a comprehensive analytical model of the heat transfer in a cross-flow multistage fluidized bed heat exchanger for particle receiver solar power plants. The model enables a parametric analysis of the heat exchanger performance to be conducted as a function of the operating conditions of the power block, the heat exchanger geometry and the fluidized bed properties. Other studies were concerned with the potential application of PCMs in high-temperature energy capture and storage, using a circulating fluidized bed (CFB) as transfer/storage mode [10]. Fornarelli et al. [11] developed a CFD model for investigating the melting process in a shell-and-tube latent heat storage with PCM for CSP applications.

Recent work has identified moving packed-bed particle heat exchangers as low-cost alternatives to fluidized beds because moving packed-beds avoid the high-cost components in fluidized beds, which include pumps to fluidize the particles and recuperators to prevent large thermal loss from the fluidization gas. Baumann et al. [12] developed a CFD multiphase model approach to describe the flow distribution and the thermal performance of a moving bed heat exchanger. They compared the numerically estimated heat transfer coefficient with the empirical penetration model, and concluded that the multiphase approach is well suited to predict the thermal behavior. Bartsch et al. [13] developed a continuous model approach, based on the theory of soil mechanics to describe the granular flow inside the heat exchanger, which was validated with particle image velocimetry (PIV) measurements of horizontal tubes. The Eulerian-Eulerian model captured the velocity profile around the tubes except for in the void region below the tube. Despite this inaccuracy, they concluded that the model is suitable for simulating moving packed beds. Isaza et al. [14] presented an analytical solution for counter-current parallel-plate moving bed heat exchangers in steady-state, applicable in sizing and thermal performance analysis. Albrecht et al. [15] developed a single-component continuum model of a moving packed-bed heat exchanger for steady state operations, capable of investigating the design trade-offs in particle size, operating temperature, and particle velocity (residence time).

For a particle-based CSP plant to be dynamically dispatched, the transient operation and control must be studied. Iverson et al. [16] studied the behavior of developmental Brayton turbomachinery in response to a fluctuating thermal input, which was varied by 50% and 100% for short durations while the system power and conditions were monitored. They concluded that, despite these fluctuations, the thermal mass in the system effectively enables the Brayton cycle to continue to run for short periods until the thermal input can recover. Samanes et al. [17] presented a transient cavity receiver model and an adaptive control able to predict the dynamic response of the receiver for different operating points. Najafabadi et al. [18] proposed an optimal dynamics and control strategy for a receiver, assessing the performance of a novel method based on aperture size adjustment in comparison to feedstock

flow adjustment, and they concluded that change in aperture size influences the system dynamics more effective than the change in gas flowrate. Studies in the literature have addressed the transients and control of liquid-liquid, liquid-gas, and gas-gas heat exchangers. Al-Dawery et al. [19] studied the transient response and control of water-water plate heat exchanger, whereas Horst et al. [20] developed a mathematical model to study the dynamic response and control strategies of and evaporator designed for automotive waste heat recovery systems. Taler [21] presented a method for numerical modeling of liquid-gas tubular cross-flow heat exchangers, which can be implemented in control systems. However, to the authors' knowledge, the dynamic analysis of a moving packed-bed particle-to-sCO_2 heat exchanger has not been published in the literature. The transients of the particle-to-sCO_2 heat exchanger are unique because of significantly higher thermal capacitance of heat-transfer material required to contain sCO_2 pressures and the large difference between the velocity of the particles and sCO_2 contained in the parallel plates. Thus, a transient model capturing the physics of the sCO_2 heat addition process from a moving packed bed of particles is necessary to enable control system design and assess turndown and ramping capabilities.

Even though control studies for particle-based CSP driving sCO_2 cycles are not found in the literature, relevant work on the dynamics and control of gas-fired and solar-assisted sCO_2 cycles have been reported on. The transient modeling and control of the gas-fired recompression Brayton cycle was recently addressed by Zitney and Liese [22] where the approach of using heat input turndown through natural gas flow rate while controlling the sCO_2 cycle using inventory, flow split, and flow rate control was detailed. Turndown of up to 93% was achieved while maintaining cycle efficiencies above 40% for turndown of up to 70%. In a follow-on publication [23], the ramping capability of the cycle was addressed where targets of 3%/min were determined to be attainable. Recently, the operational flexibility [24], control [25], and startup [26] of a solar-assisted sCO_2 cycle was address by Luu et al. Their analysis focused on the baseload operation of a partially solar heated sCO_2 cycle using direct heating of the sCO_2 in a solar receiver. Control of the cycle in response to fluctuations in the solar thermal resource was the primary concern and a control approach was detailed for the efficient operation of the cycle in off-design conditions to minimize the amount of fossil fuel usage. In CSP configurations other than direct sCO_2 receivers, the power cycle is decoupled from the solar thermal resources through the use of thermal energy storage and operating strategies other than baseload are highly valued.

In this study, a physically-based transient model of a moving packed-bed of particles and counter-flow sCO_2 fluid in a shell-and-plate configuration is presented for investigating the control and transient operation of the power generation side of a particle-based CSP plant. The aim of the particle-to-sCO_2 heat exchanger is to raise the sCO_2 temperature to 700 °C at a pressure of 20 MPa regardless of mass flow rate (thermal duty) while cooling the particles to a constant temperature of 570 °C. The model presented in this work provides a dynamic control system that enables transient analysis of the moving packed-bed particle-to-sCO_2 heat exchanger for particle-based CSP applications.

3. Modeling approach

3.1. Problem description

The model developed in this work solves the transient heat transfer problem between a moving packed-bed of particles and counter-flow sCO_2 fluid in a shell-and-plate configuration. As shown in Figure 1, particles from the hot storage tank (775 °C) enter the top of the heat exchanger and move under the force of gravity through the heat exchanger before flowing in to the cold storage tank (570 °C), where they are conveyed back to the receiver. The sCO_2 stream from the recuperative heat exchanger (550 °C) enters the heat exchanger from the bottom and is heated to 700 °C by the moving packed-bed of particles before entering the power cycle turbine. As shown in Figure 1, the sCO_2 and particles are in cross-flow configuration within the individual banks, and the flow configuration between the banks is in counter-flow. The model developed in this work assumes that the packed-bed of particles and sCO_2 stream are in a one-dimensional counter-flow configuration.

Within a moving packed-bed heat exchanger, the particles remain at or near their packing limit while flowing over the heat transfer surface. The heat transfer on the particle side is fundamentally limited by the bulk effective thermal conductivity of the granular material since cross-channel mixing doesn't occur. Analytical solutions for the particle side heat transfer coefficient have been reported in the literature [15], which result in Nusselt numbers of 9.87 and 12.0 for constant temperature and heat flux boundary conditions, respectively. The thermal conductivity of the packed bed of granular material can be determined from experimentally measured values (0.2-0.4 W/(m^2-K)) for bauxite particles in the literature [27]. Therefore, particle side heat transfer coefficient greater than 150 W/(m^2-K) should be attainable.

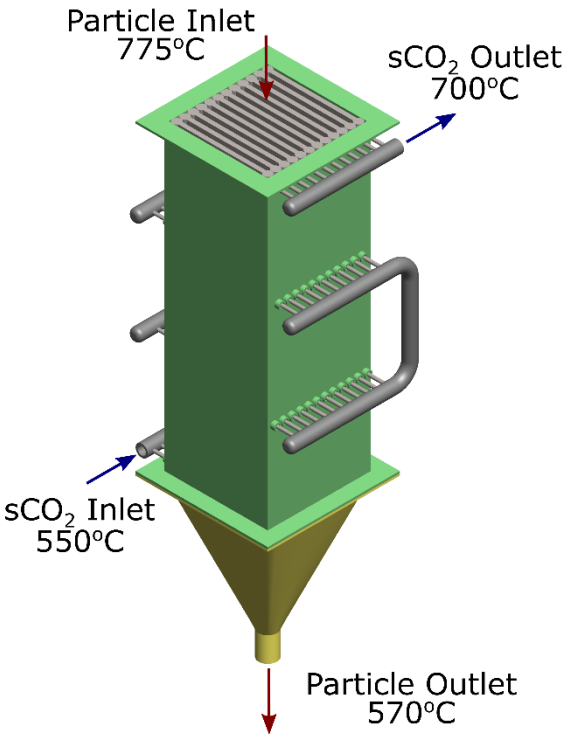

Figure 1. Illustration of a moving packed-bed particle-to-sCO_2 heat exchanger in a shell-and-plate configuration.

The single component continuum model considers the solid particulate phase to be a continuous, homogeneous and isotropic medium. Both the moving packed-bed of particles and sCO_2 stream are assumed to be one dimensional in the flow direction and transverse temperature gradients are captured through convection coefficients. The physical properties selected for the particles, which are shown in Table 1, were taken from experimental studies on particulate materials for CSP application. Particle thermal conductivity and bulk voidage were taken from Baumann et al. [27], particle specific heat was measured by Siegel et al. [28], and bulk particle density was taken from Siegel et al. [29]. The thermodynamic and transport properties of sCO_2 have been taken from Span et al. [30] and Vesovic et al. [31], respectively. The sCO_2 in the heat exchanger is assumed to behave in an isobaric manner at a pressure of 20 MPa.

Bulk particle density ρ_s (kg/m^3)	2000
Particle specific heat $c_{p,s}$ (J/(kg·K)	1200
Particle diamenter d_p (µm)	250
Particle thermal conductivity k_S (W/(m·K))	2
Bulk voidage (ε_s)	0.4
Plate density ρ_w (kg/m^3)	8238
Plate specific heat $c_{p,w}$ (J/(kg·K)	468

Table 1. Physical properties of particulate and heat exchanger material.

The simulation geometry was taken from the moving packed-bed particle-to-sCO_2 heat exchanger study conducted by Albrecht et al. [15], which considered a moving packed-bed with a height of 1 m and a width of 50 cm, so that the total heat transfer area per channel is 1.0 m^2. The space between plates of the moving packed-bed channels is set to 6 mm, which is

24 particle diameters and should be sufficient to prevent bridging. The counter-flow sCO_2 channel is 0.5 mm in width, which has been chosen to maintain the flow in a turbulent regime. At the design point, particle velocity is set to 3.4 mm/s to achieve an outlet temperature of 570 °C for a 775 °C inlet temperature, while sCO_2 velocity is set to 0.54 m/s to achieve an outlet temperature of 700 °C for a 550 °C inlet temperature. Table 2 summarizes the design parameters of the heat exchanger considered in this work.

Heat exchanger height, H (m)	1
Heat exchanger width, W (m)	0.5
sCO2 channel width, hc_{CO2} (mm)	0.5
Packed-bed channel plate spacing, hc_S (mm)	6
Plate thickness, t_{HX} (mm)	1
sCO2 velocity u_{CO2} (m/s)	0.54
Particle velocity u_s (mm/s)	3.4
sCO2 inlet temperature, $T_{in,CO2}$ (°C)	550
sCO2 outlet temperature, $T_{out,CO2}$ (°C)	700
Particles inlet temperature, $T_{in,s}$ (°C)	775
Particles outlet temperature, $T_{out,s}$ (°C)	570

Table 2. Design parameter of the heat exchanger.

3.2. Governing equations

The transient conservation-of-energy equations for the moving packed-bed of particles, sCO_2 fluid, and heat exchanger wall are solved simultaneously to determine the instantaneous temperature distributions. The moving packed-bed, sCO_2 flow and heat exchanger wall energy transport are governed by the following conservation equations

$$\rho_s \cdot c_{p,s} \cdot \frac{\partial T_s}{\partial t} = -\rho_s \cdot c_{p,s} \cdot u_s \cdot \frac{\partial T_s}{\partial x} + \frac{2 \cdot \overline{h_{sw}}}{hc_s} \cdot (T_w - T_s) \quad (1)$$

$$\rho_{CO_2} \cdot c_{p,CO_2} \cdot \frac{\partial T_{CO_2}}{\partial t} = -\rho_{CO2} \cdot c_{p,CO2} \cdot u_{CO2} \cdot \frac{\partial T_{CO_2}}{\partial x} + \frac{2 \cdot h_{CO_2}}{hc_{CO_2}} \cdot \left(T_w - T_{CO_2}\right) \quad (2)$$

$$\rho_w \cdot c_{p,w} \cdot \frac{\partial T_w}{\partial t} = \frac{\overline{h_{sw}}}{t_{HX}} \cdot (T_s - T_w) + \frac{h_{CO_2}}{t_{HX}} \cdot \left(T_{CO_2} - T_w\right) \quad (3)$$

where ρ_s, $c_{p,s}$, u_s, and T_s are the bulk particle density, particle specific heat, packed-bed velocity and particle temperature, respectively, ρ_{CO2}, $c_{p,CO2}$, u_{CO2}, and T_{CO2} are sCO_2 density, sCO_2 specific heat, sCO_2 velocity and sCO_2 temperature, respectively, and ρ_w, $c_{p,w}$, and T_w are wall density, wall specific heat and wall temperature, respectively. Thermophysical properties of the moving packed bed and sCO_2 are assumed to be constant, and sCO_2 properties are evaluated at the mean particle and sCO_2 temperature at the inlet. hc_s and hc_{CO2} are the packed-bed channels and sCO_2 channel widths, respectively. h_{CO2} is the sCO_2-to-wall heat transfer coefficient, which was obtained using the Gnielinski correlation [32] based on the hydraulic diameter, which is

twice the sCO_2 channel width. The value of h_{CO2} obtained at the design point is 600 W/(m^2·K). $\overline{h_{sw}}$ is the mean particle-to-wall heat transfer coefficient, which is assumed to be 150 W/(m^2·K) based on previous two-dimensional steady state calculations accomplished by Albrecht el al. [15]. Figure 2 shows the illustration of the shell-and-plate particle-to-sCO_2 heat exchanger model.

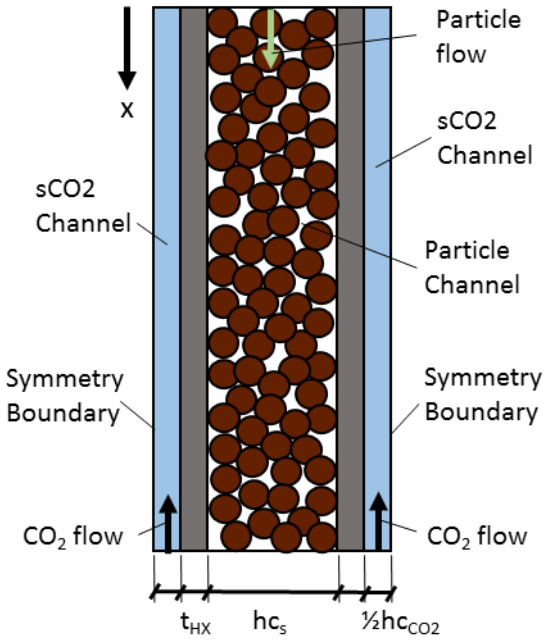

Figure 2. Illustration of the shell-and-plate packed-bed particle-to-sCO_2 heat exchanger model.

The solution of the coupled partial differential equations defining the heat exchanger model is obtained through a method-of-lines approach where a spatial discretization is imposed to turn the model into a system of coupled ordinary differential equations. The model was developed in MATLAB, making use of the internal ordinary differential equation solver ODE15s for integrating the ordinary differential equations through time. The spatial discretization was accomplished using a finite difference method for the height of the heat exchanger, with a first-order upwind scheme for the first derivative terms of particles, sCO_2 and wall temperatures. Therefore, one ordinary differential equation is obtained for each node (particle, sCO_2, heat exchange material) considered in the axial direction, which can be solved by the MATLAB solver.

Both code and solution verifications were carried out to assess the numerical accuracy of the computational simulations, independent of the physical accuracy that is the subject of validation. Model validation is accomplished by comparing a simulation result with an appropriate experimental result for specified variables at a certain set of conditions [33]. To the authors' knowledge, the dynamic analysis of a moving packed-bed particle-to-sCO_2 heat exchanger is not found in literature and the experimental data for model validation is not available. Thus, code verification and solution verification are presented in this work. Code verification is defined as a set of methods developed to find coding mistakes, whereas solution

verification is used to estimate the numerical uncertainty of a numerical solution due to numerical error (u_{num}) [33]. To carry out the verification of the transient response, outlet temperatures of particles and sCO_2 at a time sufficiently large for the temperature evolutions to reach steady state were chosen as the variables for verification. Code verification was evaluated with the order of accuracy test, which determines whether the discretization error is reduced at the expected rate. The observed order of accuracy is the accuracy that is directly computed from code output for a given simulation, whereas the formal order of accuracy is determined by the truncation error [34]. The formal order of accuracy for outlet temperatures of particles and sCO_2 is expected to be 1 as the derivative terms of temperature were solved using a first-order upwind scheme. When the exact solution is not known, three numerical solutions on different meshes are needed to obtain the observed order of accuracy

$$p = \frac{\ln\left(\frac{f_3 - f_2}{f_2 - f_1}\right)}{\ln r} \tag{4}$$

where f_3 is the solution on the coarse mesh, f_2 the solution of on the medium mesh, f_1 the solution of on the fine mesh, and r is the grid refinement factor, which is the ratio between the coarse and the fine element sizes. A value of 2 was chosen in this work, so mesh sizes of Δx_3=4 mm, Δx_2=2 mm and Δx_1=1 mm were considered in the axial direction, in order to obtain the three different numerical solutions. The inlet temperature of particles was set to 750 °C, inlet temperature of sCO_2 was set to 500 °C, and mass flow rate of sCO_2 was halved from the operating conditions. The observed order of accuracy obtained for the outlet temperature of the particles and sCO_2 were 0.99 and 1, respectively, which correspond to the formal order of accuracy, which means that the code accurately solves the mathematical model. The Grid Converge Index (GCI) was used to obtain the numerical uncertainty due to numerical errors. The GCI is an estimated 95% uncertainty obtained by multiplying the absolute value of the Richard Extrapolation error estimate by an empirically determined factor of safety, F_s, which was assigned a value of three for two-grid studies [33]. The GCI is defined as follows

$$GCI = \frac{F_s}{r^p - 1}\left|\frac{f_2 - f_1}{f_1}\right| \tag{5}$$

The GCI or expanded uncertainty $U_{95\%}$ obtained for the outlet temperature of particles and sCO_2 were 0.03% and 0.01%, respectively. Numerical standard uncertainty is obtained from GCI as follows

$$u_{num} = \frac{GCI}{k} \tag{6}$$

where the expansion factor k should be taken as 1.15 according to [33]. So the numerical uncertainty for the outlet temperature of particles and sCO_2 were 0.48 °C and 0.2 °C, which means that the real value of the outlet temperature of particles and sCO_2 were

580.887±0.48°C and 709.81±0.2°C. Another calculation on a finer mesh of Δx=0.5 mm was carried out, obtaining the values of 581.16 °C and 709.93 °C for outlet temperature of particles and sCO_2, respectively, which are within the bounds provided by the numerical uncertainty.

In this work, a measure of the sensitivity (sensitivity coefficients) of both particles and sCO_2 outlet temperatures to changes in particle-to-wall and sCO_2-to-wall heat transfer coefficients were accomplished. The procedure is to run the simulation with nominal values of heat transfer coefficients, and compare the results with those obtained with a perturbed value of heat transfer coefficients. A nominal value of 150 W/m^2K was selected for particle-to-wall heat transfer coefficient and the sCO_2-to-wall heat transfer coefficient was computed using the Gnielinski correlation [32]. The scaled sensitivity coefficients for both the sCO_2 and particle outlet temperature to variations in sCO_2-to-wall and particle-to-wall heat transfer coefficients are computed as $s = h\frac{\partial T}{\partial h}$, where the derivative is computed as a finite difference approximation in parameter space. Relative perturbation sizes ($\Delta h_{CO2}/h_{CO2}$ and $\Delta h_{sw}/h_{sw}$) selected for obtaining the sensitivity coefficients were 10, 1, 0.1, and 0.01%. Scaled sensitivity coefficients for sCO_2 outlet temperature to variations in sCO_2-to-wall and particle-to-wall heat transfer coefficients were 8 and 16 °C, respectively, whereas scaled sensitivity coefficients for particle outlet temperature to variations in sCO_2-to-wall and particle-to-wall heat transfer coefficients were 6 and 12 °C, respectively.

4. Impact of perturbations

Due to the need for a dynamic dispatch operating strategy, the transient response of the heat exchanger to changes in the thermal demand of the power cycle must be studied. In addition, variations in solar flux, heat loss from the high-temperature storage tank, and power cycle heat rejection temperature result in inlet temperature disturbances that have to be accommodated. Therefore, models should be able to predict the dynamic characteristics of the heat exchanger for variations in inlet and operating conditions. A control strategy is required to maintain a relatively constant particle outlet and sCO_2 turbine inlet temperature provided by the heat exchanger for varying conditions; however, this problem has yet to receive attention for the application of particle-based CSP plants.

The primary objective of this work is to observe the heat exchanger response to perturbations in operating conditions, thereby simulating a potential transient experienced during dynamic dispatch operation. Table 3 summarizes the changes introduced in inlet temperatures of particles, inlet temperature of sCO_2 and mass flow rate of sCO_2 in order to study the transient response of the heat exchanger.

	$T_{in,s}$ (°C)	$T_{in,CO2}$ (°C)	m_{CO2} (kg/s)
Design point	775	550	0.0267
1	725	500	0.0133
2	750	550	0.0133
3	775	500	0.0133
4	775	550	0.0133
5	750	500	0.0267
6	775	500	0.0267

Table 3. Variations from the design point ($T_{in,s}$=775 °C, m_s=0.02 kg/s, T_{sCO2}=550 °C, m_{sCO2}=0.0267 kg/s) introduced in inlet temperature of particles and sCO_2, and mass flow of sCO_2, for the six different cases considered in this work.

For each previous case, the boundary conditions for the differential equations can be expressed as

$$T_{CO2}(t, x = H) = T_{in,CO2} \tag{7}$$

$$T_s(t, x = 0) = T_{in,s} \tag{8}$$

4.1. Transient response of the heat exchanger without control

The simulations were carried out for two different rates of change in the inlet conditions, which correspond to instantaneous changes (step change), and linear changes (ramp) over a 30 minute interval. For cases one to six, the transient response of the heat exchanger without control for instantaneous changes in inlet conditions are shown in Figure 3, while Figure 4 shows the transient response when inlet conditions vary linearly over a 30 minute interval. As shown in Figure 3 (d), outlet temperature of sCO_2 (turbine inlet temperature) increases with reductions in sCO_2 mass flow rate (cases one to four). The reduction in sCO_2 mass flow rate represents 50% turndown in the thermal input to the power cycle. The sCO_2 turbine inlet temperature increase is the result of a reduction in the thermal capacitance of the cold fluid. For cases one and two, the increase in sCO_2 outlet temperature is lower due to the simultaneous reduction in inlet temperature of the particles. The outlet temperature of sCO_2 is reduced when the sCO_2 mass flow rate is kept constant and inlet temperature of sCO_2 decreases by 50 °C (cases five and six). The sCO_2 outlet temperature reduction is stronger when both sCO_2 and particle outlet temperatures are decreased (case five). As shown in Figure 3 (e), particles outlet temperature profiles follow the same trend as sCO_2 outlet temperature profiles, except for cases one and three, where both mass flow rate and inlet temperature of sCO_2 are reduced. In these cases, the particle outlet temperature first decreases due to the reduction in sCO_2 inlet temperature, and then increases due to the reduction in thermal capacitance of the sCO_2.

Comparing Figures 3 and 4, both sCO_2 and particle outlet temperature profiles follow the same trend. However, slower changes in sCO_2 and particle outlet temperature are experienced when inlet conditions vary linearly over a 30 minute interval. Regardless of the rate of change, large deviations from the desired setpoints are experienced in the particle outlet temperature and

sCO_2 turbine inlet temperature. The maximum deviation in the particle outlet and sCO_2 turbine inlet temperature is 60 °C for the six cases presented here.

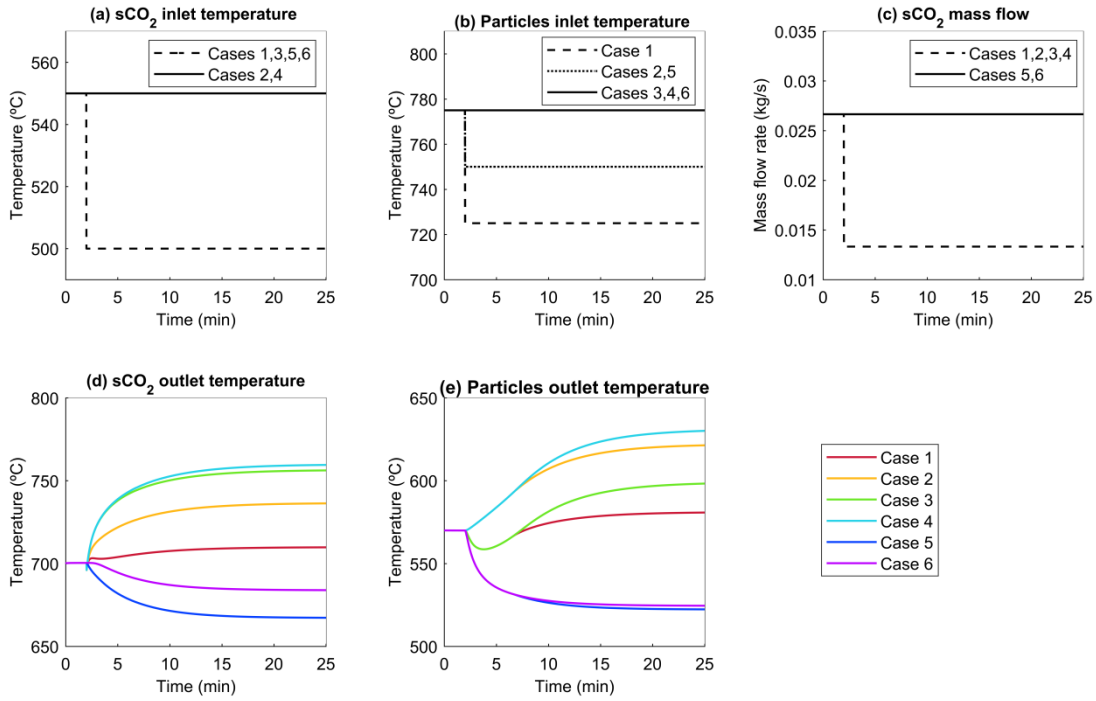

Figure 3. Transient response of the heat exchanger for the six different cases considered, when inlet conditions vary instantaneously. (a), (b) and (c) show the changes introduced in inlet conditions, while (d) and (e) show outlet temperature profiles of sCO_2 and particles.

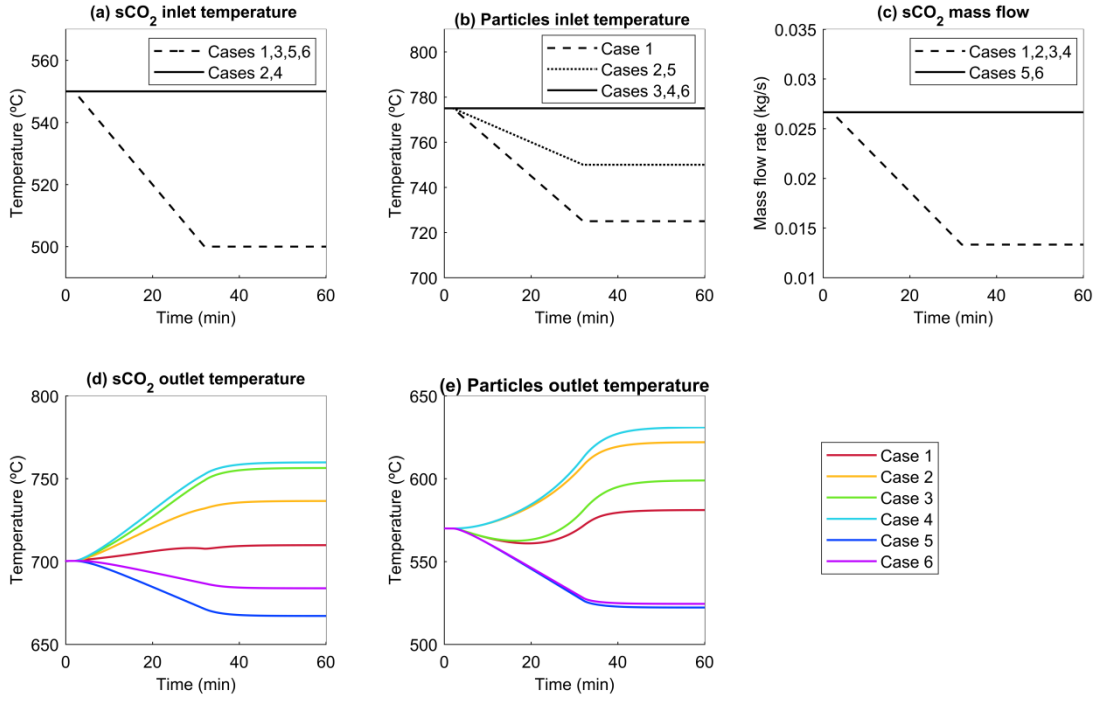

Figure 4. Transient response of the heat exchanger for the six different cases considered, when inlet conditions vary linearly along 30 minutes. (a), (b) and (c) show the changes introduced in inlet conditions, while (d) and (e) show outlet temperature profiles of sCO_2 and particles.

5. Control strategies

As shown in the previous section, a control system is needed to maintain the desired sCO_2 turbine inlet temperature and particle outlet temperature of 700 °C and 570 °C, respectively. The control system developed in this work is based on adjusting particle and sCO_2 flow rate to produce the desired sCO_2 and particle outlet temperatures. Heat exchangers in steady state operation are governed by the overall heat exchanger energy balance equation,

$$m_{CO2,HX} \cdot c_{p,CO2} \cdot (T_{out,CO2,HX} - T_{in,CO2}) = m_s \cdot c_{p,s} \cdot (T_{in,s} - T_{out,s}) \quad (9)$$

and relationship between the overall heat transfer coefficient, heat transfer area, and log mean temperature difference,

$$m_s \cdot c_{p,s} \cdot (T_{in,s} - T_{out,s}) = U \cdot A \cdot \Delta T_{lm} \quad (10)$$

where $m_{s,CO2,HX}$ and m_s are the mass flow rates of sCO_2 and particles, respectively. $T_{in,s}$ is the inlet temperature of particles, $T_{out,s}$ is the outlet temperature of particles, $T_{in,CO2}$ is the inlet temperature of sCO_2 ,$T_{out,CO2,HX}$ is the outlet temperature of sCO_2, A is the area of the heat exchanger, U is the overall heat transfer coefficient, calculated as

$$U = \left(\frac{1}{\overline{\overline{h_{sw}}}} + \frac{t_{HX}}{k_{HX}} + \frac{1}{h_{CO2}} \right)^{-1} \quad (11)$$

and ΔT_{lm} is the log mean temperature difference calculated as

$$\Delta T_{lm} = \frac{\left(T_{out,s} - T_{in,CO2}\right) - \left(T_{in,s} - T_{out,CO2,HX}\right)}{\ln \frac{T_{out,s} - T_{in,CO2}}{T_{in,s} - T_{out,CO2,HX}}} \quad (12)$$

For a given particle-to-sCO_2 heat exchanger design, the area of the heat exchanger and overall heat transfer coefficient are assumed to be fixed. The mass flow rate of sCO_2 is prescribed by the thermal duty required by the power block. Therefore, the mass flow rate of the particles is the only variable that can be adjusted to maintain both the sCO_2 turbine inlet temperature and particle outlet temperature. Therefore, it is not possible to obtain the desired outlet

temperature of sCO_2 and particles by only varying the particles mass flow through the heat exchanger.

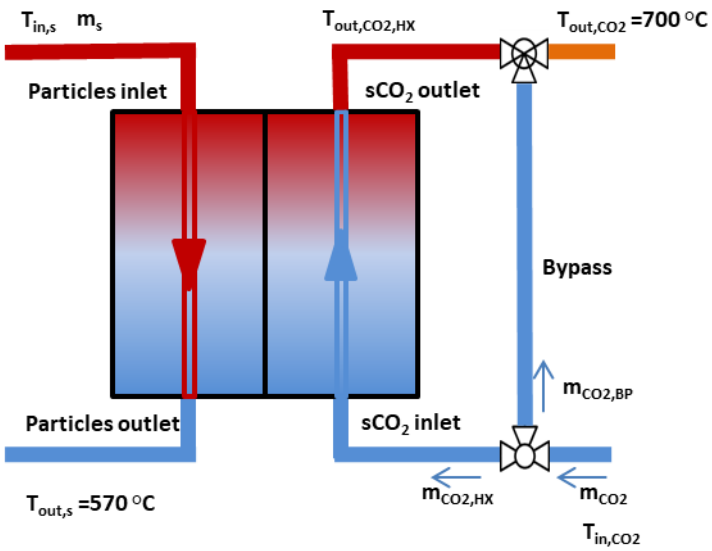

Figure 5. Schematic diagram of the control system of the particle-to-sCO_2 heat exchanger proposed, including the separating valve and the mixer.

The control system presented in this work consists of a split valve in the sCO_2 stream, so that the sCO_2 mass flow is divided in two streams, one of them flowing through the heat exchanger, and another flowing outside the heat exchanger (bypass), as shown in Figure 5. Once the sCO_2 stream leaves the heat exchanger, both sCO_2 streams are mixed before entering the power block turbine. Therefore, the total sCO_2 mass flow is prescribed by the thermal requirements of the power block, but the fraction that is diverted around the heat exchanger can be adjusted to obtain the desired outlet temperatures. When the split valve and mixer are installed in the sCO_2 stream, two more equations are added to the system, which are the mass balance in the mixer

$$m_{CO2} = m_{CO2,BP} + m_{CO2,HX} \tag{13}$$

and the energy balance in the mixer

$$m_{CO2} \cdot c_{p,CO2} \cdot T_{out,CO2} = m_{CO2,HX} \cdot c_{p,CO2} \cdot T_{out,CO2,HX} + m_{CO2,BP} \cdot c_{p,CO2} \cdot T_{in,CO2} \tag{14}$$

where $m_{CO2,BP}$ is the sCO_2 stream flowing outside the heat exchanger, $m_{CO2,HX}$ is the sCO_2 stream flowing through the heat exchanger, $T_{out,\ CO2,HX}$ is the outlet temperature of the sCO_2 stream

flowing through the heat exchanger, and $T_{out,CO2}$ is the temperature of the sCO_2 entering the power block, once the two streams have been mixed.

Considering the steady state operation of the heat exchanger, for the prescribed inlet temperatures of sCO_2 and particles, and prescribed sCO_2 mass flow rate by the power block, both the sCO_2 and particle mass flow rates through the heat exchanger can be adjusted to meet the desired outlet temperatures. The system of equations is defined by Equations (4), (5), (8) and (9), to determine four unknown variables: $m_{CO2,BP}$, $m_{CO2,HX}$, $T_{out,CO2,HX}$ and m_s.

The steady state solution of both the sCO_2 and particle mass flow rates through the heat exchanger for the six different cases previously studied are shown in Table 4, which result in the desired particle outlet and sCO_2 turbine inlet temperature.

	$T_{in,s}$ (°C)	$T_{in,CO2}$ (°C)	m_{CO2} (kg/s)	$m_{CO2,HX}$ (kg/s)	m_s (kg/s)
1	725	500	0.0133	0.0129	0.0178
2	750	550	0.0133	0.0126	0.0115
3	775	500	0.0133	0.0110	0.0135
4	775	550	0.0133	0.0115	0.0101
5	750	500	0.0267	0.0258	0.0307
6	775	500	0.0267	0.0233	0.0270

Table 4. Steady state solution of sCO_2 and particles mass flow rates through the heat exchanger for the six different cases previously studied.

5.1. Feed-forward control strategy

The control system of the particle-to-sCO_2 heat exchanger can be developed based on sCO_2 and particle mass flow rates obtained from the steady state solutions calculated at each instant in time. The steady state solution can be calculated from the measured inlet temperatures of sCO_2 and particles, as well as the total sCO_2 mass flow rate required by the power block. Therefore, the particle mass flow rate evolution with time can be obtained by Equation (10), which is the steady state overall energy balance.

$$m_{s,f-f}(t) = \frac{c_{p,CO2} \cdot m_{CO2}(t) \cdot (T_{out,CO2} - T_{in,CO2}(t))}{c_{p,s} \cdot (T_{in,s}(t) - T_{out,s})} \quad (15)$$

where $m_{s,f\text{-}f}$ is the particles mass flow rate based on the steady state solution, $T_{out,CO2}$ is the desired sCO_2 outlet temperature (700 °C), and $T_{out,s}$ is the desired particles outlet temperature (570 °C). The other unknown variable is the sCO_2 mass flow through the heat exchanger. The solution of the steady state model with a fixed conductance can specify the sCO_2 flow rate based on inlet conditions. For the purposes of the transient simulations conducted in the

following sections, which run much faster than real time, the steady state solutions have been fit to polynomial functions of the inlet conditions that undergo changes. For cases one to four, where sCO_2 mass flow rate required by the power block is reduced by half, sCO_2 mass flow rate through the heat exchanger can be obtained as a function of total sCO_2 mass flow rate by Equation (11)

$$m_{CO2,HX,f-f}(t) = a \cdot {m_{CO2}}^4\,(t) + b \cdot {m_{CO2}}^3\,(t) + \mathrm{c} \cdot {m_{CO2}}^2\,(t) + \mathrm{d} \cdot m_{CO2}\,(t) + \mathrm{e} \qquad (16)$$

where $m_{CO2,HX,f-f}$ is the sCO_2 mass flow through the heat exchanger based on the steady state solution. For cases five and six, where thermal duty does not experience changes from the design point, sCO_2 mass flow rate through the heat exchanger can be obtained as a function of inlet temperature of particles and sCO_2, respectively.

$$m_{CO2,HX,f-f}(t) = a \cdot {T_{in,s}}^4\,(t) + b \cdot {T_{in,s}}^3\,(t) + \mathrm{c} \cdot {T_{in,s}}^2\,(t) + \mathrm{d} \cdot T_{in,s}\,(t) + \mathrm{e} \qquad (17)$$

$$m_{CO2,HX,f-f}(t) = a \cdot {T_{in,CO2}}^4\,(t) + b \cdot {T_{in,CO2}}^3\,(t) + \mathrm{c} \cdot {T_{in,CO2}}^2\,(t) + \mathrm{d} \cdot T_{in,CO2}\,(t) + \mathrm{e} \qquad (18)$$

where parameters a, b, c, d and e are constants fit to the steady state solution of sCO_2 mass flow through the heat exchanger, and are shown in Table 5.

	a	b	c	d	e
1	2.411040E+05	-1.647343E+04	4.270827E+02	-4.124407	2.341261E-02
2	2.090366E+04	-1.672939E+03	6.471468E+01	-1.984076E-01	7.096486E-03
3	3.477962E+05	-2.435447E+04	6.596516E+02	-7.267684	3.735256E-02
4	4.482453E+04	-3.465941E+03	1.270049E+02	-1.225268	1.209379E-02
5	1.1510258E-08	-3.4843931E-05	3.9556664E-02	-1.9959499E+01	3.7768923E+03
6	8.235577E-10	-1.691923E-06	1.304004E-03	-4.468377E-01	5.745914E+01

Table 5. Constants a, b, c, d, e of Equations 11, 12 and 13, for the six different cases considered.

Figure 6 and Figure 7 show the particle outlet and sCO_2 turbine inlet temperature when the feed-forward control system proposed in this work is applied compared to those when no control is used, for the six different cases previously studied. Figure 6 shows the comparison when changes in the inlet conditions occur instantaneously, whereas Figure 7 shows the results obtained for linear changes in the inlet conditions over a 30-minute interval. As shown in Figure 6 (a), applying the feed-forward control strategy results in initial temperature deviations from the desired 700 °C sCO_2 turbine inlet temperature. However, the presence of the sCO_2 bypass and adjustment of the flow rates based on the steady-state model are able to return the sCO_2 turbine inlet temperature and particle outlet temperature to the setpoints. The maximum initial sCO_2 temperature deviation is 44 °C when both mass flow rate and inlet temperature of sCO_2 are reduced (case three), and the maximum settling time is approximately 20 minutes for the sCO_2 turbine inlet temperature to achieve a value of 700±1

°C. The maximum particle outlet temperature deviation from the desired 570 °C is 20 °C for case three.

The feed-forward control strategy results obtained for linear changes in the inlet conditions, which occur over a 30-minute interval, are plotted in Figure 7. Figure 7 (a) and (b) show that the outlet temperature deviations of sCO_2 and particles are lower when changes in inlet conditions occur over 30 minutes. The maximum sCO_2 and particle outlet temperature deviations from the desired point are 5 °C and 7 °C, respectively. Therefore, the feed-forward control strategy based on the steady state model is applicable for gradual perturbations in the inlet conditions and thermal duty.

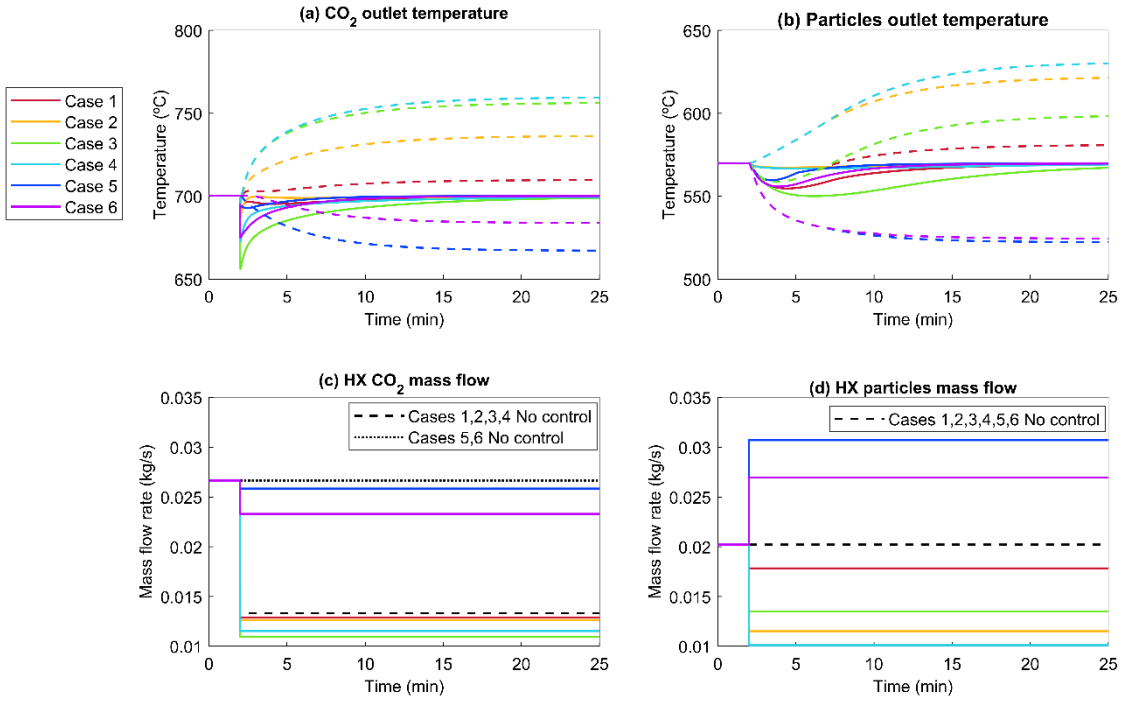

Figure 6. Comparison between the heat exchanger response obtained applying feed-forward control and not applying any control for the six different cases considered, when inlet conditions vary instantaneously. (a) and (b) show the outlet temperature profiles of sCO_2 and particles when feed-forward control is applied (solid lines), compared with those without any control applied (dashed lines). (c) and (d) show the evolution with time of sCO_2 and particles mass flow rates based on feed-forward control (solid lines), and those without any control applied (black dashed and dotted lines).

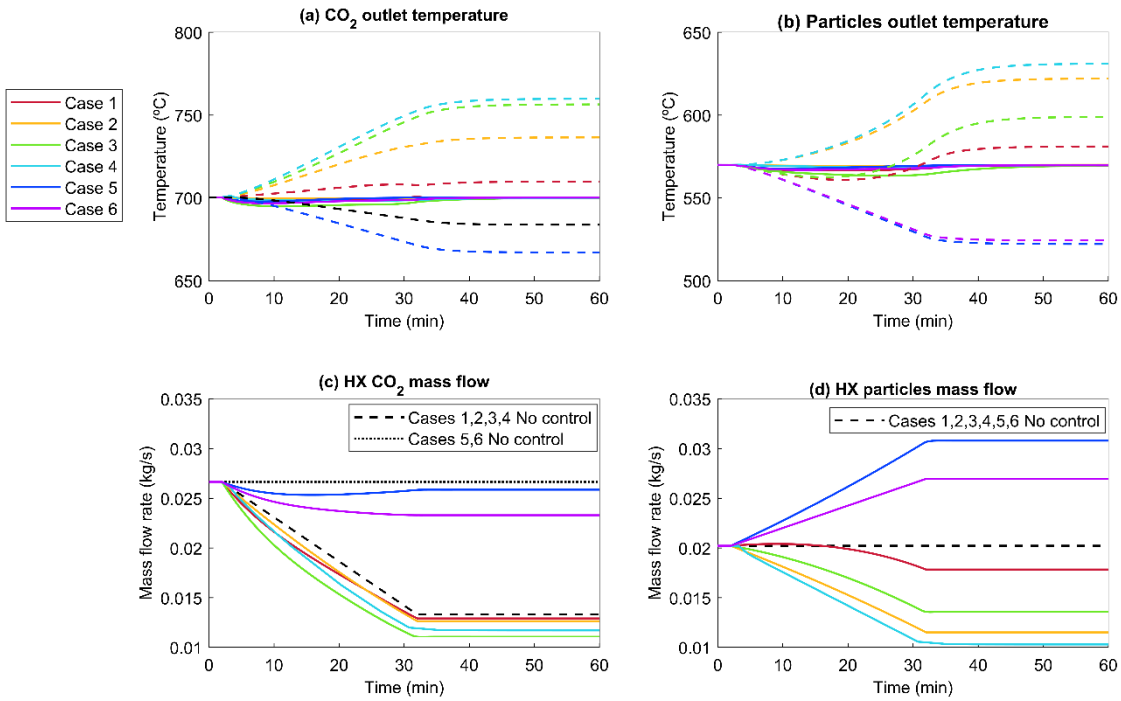

Figure 7. Comparison between the heat exchanger response obtained applying feed-forward control and not applying any control for the six different cases considered, when inlet conditions vary linearly along 30 minutes. (a) and (b) show the outlet temperature profiles of sCO_2 and particles when feed-forward control is applied (solid lines), compared with those without any control applied (dashed lines). (c) and (d) show the evolution with time of sCO_2 and particles mass flow rates based on feed-forward control (solid lines), and those without any control applied (black dashed and dotted lines).

5.2. Feedback control strategy

As shown in the previous subsection, temperature deviations of sCO_2 and particles obtained for the feed-forward control strategy are not admissible for instantaneous changes in the inlet conditions. Therefore, a feedback control strategy based on a combination of the steady-state solution used in the feed-forward control strategy and a correction by both sCO_2 and particle outlet temperature deviations was developed to reduce both temperature deviations and time to reach the desired temperature. Mass flow rates of particles and sCO_2 can be obtained by Equations (14) and (15), respectively

$$m_{s,f-b}(t) = m_{s,f-f}(t) \; - \; K_s \cdot (T_{out,p}(t) - 570) \tag{19}$$

$$m_{CO2,HX,f-b}(t) = m_{CO2,HX,f-f}(t) \; - \; K_{CO2} \cdot (T_{out,sCO2}(t) - 700) \tag{20}$$

where $m_{p,f\text{-}b}$ and $m_{sCO2,HX,f\text{-}b}$ are particles and sCO_2 mass flow rates obtained in the feedback control strategy, respectively. Table 6 shows the values of K_s and K_{CO2}, which are proportional constants that are adjusted to reduce particle and sCO_2 outlet temperature deviations.

	K_{CO2}		K_s	
	Instantaneous change	30 min change	Instantaneous change	30 min change
1	1.00E-04	5.00E-04	0.02	5.00E-03
2	1.00E-04	0	1.00E-04	0
3	1.00E-04	1.00E-04	0.1	7.00E-03
4	1.00E-04	1.00E-04	0.1	1.50E-04
5	1.00E-04	1.00E-04	0.02	7.00E-03
6	1.00E-04	1.00E-04	0.02	7.00E-03

Table 6. Constants K_{CO2} and K_s of Equations 14 and 15, for the six different cases considered when inlet conditions vary instantaneously, or linearly along 30 minutes.

Figure 8 and Figure 9 show the outlet temperature profiles of sCO_2 and particles when the feed-forward control system is applied compared to those when feedback control system is applied. As shown in Figure 8 (a) and (b), temperature deviations of the sCO_2 turbine inlet temperature from 700 °C, and temperature deviation of particle outlet from 570 °C are significantly reduced for instantaneous changes in the inlet conditions. For case three, where the total sCO_2 mass flow is reduced by one half, the temperature deviation of sCO_2 is decreased from 44 °C with the feed-forward control strategy to 16 °C with feedback control, and time to achieve the desired temperature of 700±1 °C is reduced from 20 minutes with feed-forward control to 3 minutes with feedback control. The reduction in temperature deviation of particles leaving the heat exchanger comparing feed-forward and feedback control strategies is notable too, from 20 °C for feed-forward control to 0.2 °C for feedback control.

As shown in Figure 9 (a) and (b) when inlet conditions vary linearly over a 30 minute interval, the maximum sCO_2 temperature deviation is reduced from 5 °C with feed-forward control, to 1.2 °C with feedback control, and maximum particle temperature deviation is reduced from 7 °C with feed-forward control, to 0.2 °C with feedback control.

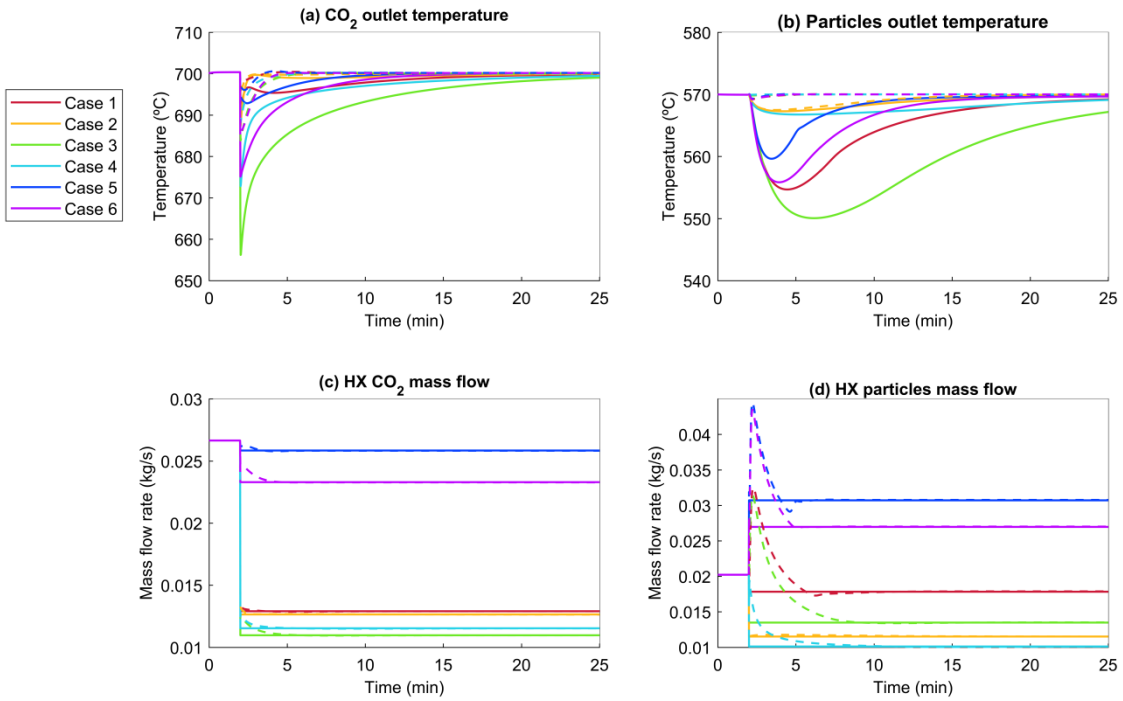

Figure 8. Comparison between the heat exchanger response obtained applying feed-forward control and feedback control for the six different cases considered, when inlet conditions vary instantaneously. (a) and (b) show the outlet temperature profiles of sCO_2 and particles when feed-forward control is applied (solid lines), compared with those when feedback control is applied (dashed lines). (c) and (d) show the evolution with time of sCO_2 and particles mass flow rates based on feed-forward control (solid lines), and those based on feedback control (dashed lines).

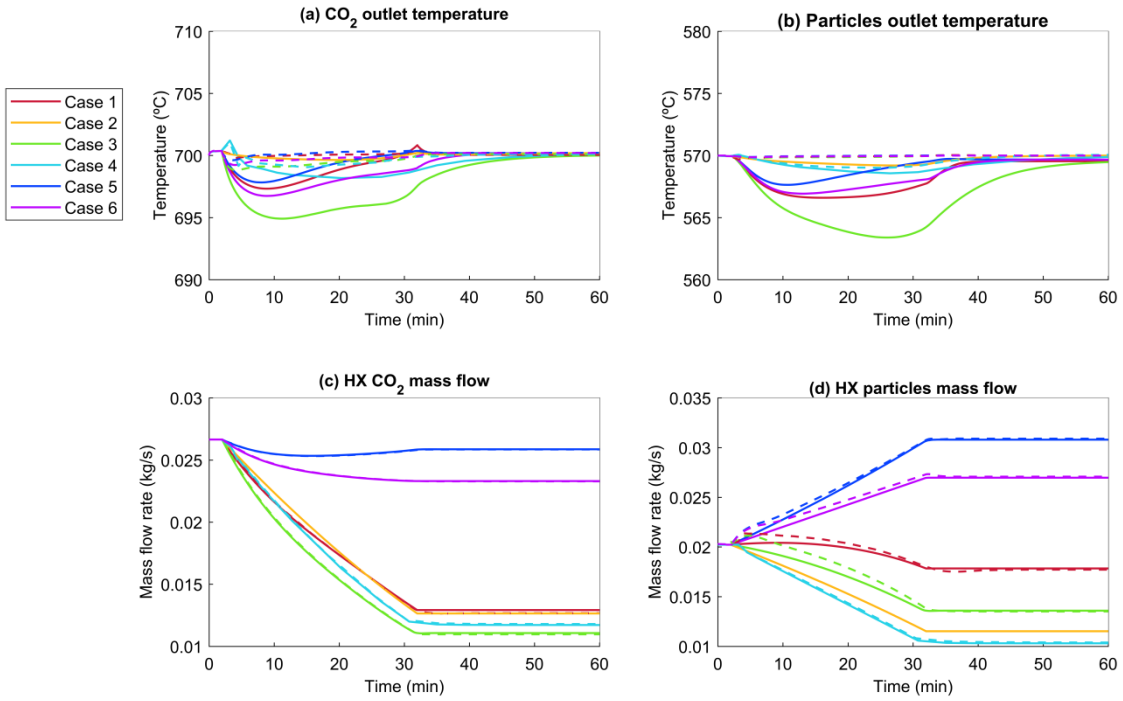

Figure 9. Comparison between the heat exchanger response obtained applying feed-forward control and feedback control for the six different cases considered, when inlet conditions vary linearly along 30 minutes. (a) and (b) show the outlet temperature profiles of sCO_2 and particles when feed-forward control is applied (solid lines), compared with those when feedback control is applied (dashed lines). (c) and (d) show the evolution with time of sCO_2 and particles mass flow rates based on feed-forward control (solid lines), and those based on feedback control (dashed lines).

6. Discussion

The operation of next-generation CSP plants will require significant turndown capabilities as well as rapid ramping to accommodate periods of diminished production from renewable generators (i.e., photovoltaics and wind) without thermal storage. To enable such an operating strategy, flexible primary heat exchangers for next-generation CSP technologies coupled to sCO_2 power cycles need to be demonstrated. Particle-based CSP is one of the leading concepts for dispatchable, high-efficiency solar electricity production. However, studies on the primary power cycle heat exchanger are limited in the literature and investigations into the ramp rate and control are nonexistent.

Current ramp rates for gas-fired sCO_2 power cycles are in the range of 3%/min [23]. However, meeting these targets for solar-driven sCO_2 cycles, which will differ in the construction of the primary power-cycle heat exchanger and use of dry cooling, have not been addressed. The control of the primary power-cycle heat exchanger for a particle-based CSP system is a key step in developing a system model for the investigation of an integrated particle-based CSP system driving an sCO_2 power cycle. The results and modeling technique presented here can be leverage in future studies to address questions surrounding the ramp rate and disturbance rejection for variations in the particle inlet temperature, which can result from heat loss in the storage bins or variations in the receiver outlet temperature.

Control of sCO_2 cycles for CSP application will most likely employ inventory control, which removes and adds sCO_2 to the system to modulate the flow rate without changing the speed of the turbomachinery. It is desirable to maintain turbine inlet temperature and rotational speed to prevent reduction in cycle thermal efficiency during turndown [22]. A rapid approach for returning the system to turbine inlet temperature at off-design conditions for a particle CSP heat source was provided here. Furthermore, the control system developed for a closed loop of particles has special considerations compared to a gas-fired cycle where the exhaust temperature is not a concern. In a closed particle loop, the particle temperature leaving the heat exchanger must be controlled such that the receiver inlet temperature is maintained at a constant value.

Future work should look to experimentally validate the heat-exchanger model. Steady-state performance and the transient response to step changes in inlet conditions should be investigated to show that the model used in this study appropriately captures the heat exchanger physics. In addition, testing of the control methodology should be investigated experimentally in a prototype unit.

7. Conclusions

In this work, the transient response of a moving packed bed particle-to-sCO2 heat exchanger to perturbations in inlet conditions and changes in thermal duty was analyzed. Six different cases varying inlet temperature of the sCO_2 and particle streams as well as sCO_2 mass flow rate required by the power block were investigated. Simulations without control displayed temperature deviations of sCO_2 entering the power block greater than 50 °C from the desired value of 700 °C. Therefore, a control system was implemented to maintain the temperature of the sCO_2 flowing into the power cycle turbine at 700 °C and the temperature of the particles leaving the heat exchanger at 570 °C during transient operation.

The control system proposed is based on installing a split valve and a mixer in the sCO_2 side, so that the sCO_2 stream is divided in two streams, one of them flowing through the heat exchanger, and another flowing outside the heat exchanger. Both streams mix before flowing through the power block at the desired temperature of 700 °C. Therefore, the desired sCO_2 turbine inlet and particle outlet temperatures can be maintained by adjusting both particle and sCO_2 mass flow rates through the heat exchanger.

Two methods of controlling the flow rates during the transient were investigated. A feed-forward control methodology was developed based on the steady-state solution of lumped heat-exchanger modeling equations and compared to feedback control where the model result was corrected by a proportional term. The maximum sCO_2 outlet temperature deviation for the case of instantaneous changes in inlet conditions was reduced from 44°C with feed-forward control to 16 °C with feedback control, and the time for sCO_2 to reach the desired 700 °C in the turbine was decreased from 20 minutes with feed-forward control, to 3 minutes with feedback control. When inlet conditions vary linearly over 30-minute intervals (as opposed to an instantaneous step change), the maximum sCO_2 outlet temperature deviation was reduced from 5 °C with feed-forward control to 1 °C with feedback control. The analysis conducted in this work illustrates the possibility of dynamically dispatching next generation particle-based CSP plants driving sCO_2 power cycles.

Nomenclature

A	area (m^2)
c_p	specific heat (J/(kg·K))
d_p	particle diameter (m)
GCI	Grid Convergence index (%)
h	heat transfer coefficient (W/(m^2·K))
hc	plate spacing (mm)
H	height (m)
k	conductivity (W/(m·K))
m	mass flow rate (kg/s)

p observed order of accuracy (-)

r refinement factor (-)

s scaled sensitivity coefficient (°C)

t time (s)

t_{HX} plate thickness (mm)

T temperature (°C)

u velocity (m/s)

u_{num} numerical uncertainty (%)

U overall heat transfer coefficient (W/(m^2·K))

W width (m)

Greek letters

ΔT_{lm} logarithm mean temperature difference (-)

ε voidage (-)

ρ density (kg/m^3)

Subscripts

BP bypass

f-b feedback control strategy

HX heat exchanger

in inlet

f-f feed-forward control strategy

out outlet

s particulate phase

w heat exchanger wall

Acknowledgements

The present work has been funded by DOE SunShot Program (SuNLaMP-0000000-1507), and the scholarship FPU14/04941 of the Spanish Ministry of Education, Culture and Sport. The

authors gratefully appreciate this support. Sandia National Laboratories is a multimission laboratory managed and operated by National Technology and Engineering Solutions of Sandia LLC, a wholly owned subsidiary of Honeywell International Inc. for the U.S. Department of Energy's National Nuclear Security Administration under contract DE-NA0003525.

References

[1] M. J. Wagner, A. M. Newman, W. T. Hamilton y R. J. Braun, «Optimized dispatch in a first-principles concentrating solar power production model,» *Applied Energy,* vol. 203, pp. 959-971, 2017.

[2] M. Mehos, C. Turchi, J. Vidal, M. Wagner, Z. Ma, C. Ho, W. Kolb, C. Andraka y A. Kruizenga, «Concentrating Solar Power Gen3 Demonstrations Roadmap,» 2017.

[3] C. K. Ho y B. D. Iverson, «Review of high-temperature central receiver designs,» *Renewable and Sustainable Energy Reviews,* vol. 29, pp. 835-846, 2014.

[4] C. K. Ho, «A review of high-temperature particle receivers for concentrating solar power,» *Applied Thermal Engineering,* vol. 109, nº 1, pp. 958-969, 2016.

[5] N. P. Siegel, C. K. Ho, S. S. Khalsa y G. J. Kolb , «Development and Evaluation of a Prototype Solid Particle Receiver: On-Sun Testing and Model Validation,» *Journal of Solar Energy Engineering,* vol. 132, nº 2, p. 021008, 2010.

[6] C. K. Ho, J. Christian, D. Gill, A. Moya , S. Jeter, S. Abdel-Khalik, D. Sadowski, N. Siegel, H. Al-Ansary, L. Amsbeck, B. Gobereit and R. Buck, "Technology advancements for next generation falling particle," *Energy Procedia,* vol. 49, pp. 398-407, 2014.

[7] H. Zhang, H. Benoit, D. Gauthier, J. Degrève, J. Baeyens, I. Pérez-López, M. Hemati y G. Flamant, «Particle circulation loops in solar energy capture and storage: Gas–solid flow and heat transfer considerations,» *Applied Energy,* vol. 161, pp. 206-224, 2016.

[8] C. S. Turchi, Z. Ma, T. W. Neises y M. J. Wagner, «Thermodynamic study of advanced supercritical carbon dioxide power cycles for concentrating solar power systems,» *Journal of Solar Energy Engineering,* vol. 135, p. 041007, 2013.

[9] F. Gomez-Garcia, D. Gauthier y G. Flamant, «Design and performance of a multistage fluidised bed heat exchanger for particle-receiver solar power plants with storage,» *Applied Energy,* vol. 190, pp. 510-523, 2017.

[10] F. Pitié, C. Y. Zhao , J. Baeyens, J. Degrève y H. L. Zhang, «Circulating fluidized bed heat recovery/storage and its potential to use coated phase-change-material (PCM) particles,» *Applied Energy,* vol. 109, pp. 505-513, 2013.

[11] F. Fornarelli , S. M. Camporeale, B. Fortunato, M. Torresi, P. Oresta, L. Magliochetti , A.

Miliozzi y G. Santo, «CFD analysis of of melting process in a shell-and-tube latent heat storage for concentrated solar power plants.,» *Applied Energy*, vol. 164, pp. 711-722, 2016.

[12] T. Baumann, S. Zunft y R. Tamme, «Moving bed heat exchangers for use with heat storage in concentrating solar plants: a multiphase model,» *Heat transfer engineering,* vol. 35, nº 3, pp. 224-231, 2014.

[13] P. Bartsch, T. Baumann y S. Zunft, «Granular flow field in moving packed bed heat exchangers: a continuous model approach,» *Energy Procedia,* vol. 99, pp. 72-79, 2016.

[14] P. A. Isaza, W. D. Warnica y M. Bussmann, «Co-current parallel-plate moving bed heat exchanger: an analytical solution,» *International Journal of Heat and Mass Transfer,* vol. 87, pp. 616-624, 2015.

[15] K. J. Albrecht y C. K. Ho, «Heat transfer models of moving packed-bed particle-to-sCO2 heat exchangers,» Charlotte, 2017.

[16] B. D. Iverson, T. M. Conboy, J. J. Pasch y A. M. Kruizenga, «Supercritical CO2 Brayton cycles for solar-thermal energy,» *Applied Energy,* vol. 111, pp. 957-970, 2013.

[17] J. Samanes y J. García-Barberena, «A model for the transient performance simulation of solar cavity receivers,» *Solar Energy,* vol. 110, pp. 789-806, 2014.

[18] H. A. Najafabadi y N. Ozalp, «Development of a control model to regulate temperature in a solar receiver,» *Renewable Energy,* vol. 111, pp. 95-104, 2017.

[19] S. K. Al-Dawery, A. M. Alrahawi y K. M. Al-Zobai, «Dynamic modeling and control of plate heat exchanger,» *International Journal of Heat and Mass Transfer,* vol. 55, pp. 6873-6880, 2012.

[20] T. A. Horst, H.-S. Rottengruber, M. Seifert y J. Ringler, «Dynamic heat exchanger model for performance prediction and control system design of automotive waste heat recovery systems,» *Applied Energy,* vol. 105, pp. 293-303, 2013.

[21] D. Taler, «Mathematical modeling and control of plate fin and tube heat exchangers,» *Energy Conversion and Management,* vol. 96, pp. 452-462, 2015.

[22] S. E. Zitney y E. A. Liese, «Dynamic Modeling and Simulation of a 10 MWe Supercritical CO2 Recompression Brayton Power Cycle for Off-Design, Part-Load, and Control Analysis,» de *6th International Supercritical CO2 Power Cycles Symposium*, Pittsburgh, 2018.

[23] P. Mahapatra, J. Albright, S. E. Zitney y E. A. Liese, «Advanced Regulatory Control of a 10 MWe Supercritical CO2 Recompression Brayton Cycle towards Improving Power Ramp Rates,» de *The 6th International Supercritical CO2 Power Cycles Symposium*, Pittsburgh, 2018.

[24] M. T. Luu, D. Milani, R. McNaughton y A. Abbas, «Analysis for flexible operation of supercritical CO2 Brayton cycle integrated with solar thermal systems,» *Energy,* vol. 124, pp. 752-771, 2017.

[25] M. T. Luu, D. Milani, R. McNaughton y A. Abbas, «Advanced control strategies for dynamic operation of a solar-assisted recompression supercritical CO2 Brayton power cycle,» *Applied Thermal Engineering,* vol. 136, pp. 682-700, 2018.

[26] M. T. Luu, D. Milani, R. McNaughton y A. Abbas, «Dynamic modelling and start-up operation of a solar assisted recompression supercritical CO2 Brayton power cycle,» *Applied Energy,* vol. 199, pp. 247-263, 2017.

[27] T. Baumann y S. Zunft, «Properties of granular materials as heat transfer and storage medium in CSP application,» *Solar Energy Materials and Solar Cells,* vol. 143, pp. 38-47, 2015.

[28] N. P. Siegel, M. D. Gross y R. Coury, «The Development of Direct Absorption and Storage Media for Falling Particle Solar Central Receivers,» *Journal of Solar Energy Engineering,* vol. 137 (4), pp. 041003–041007, 2015.

[29] N. Siegel, M. Gross, C. Ho, T. Phan y J. Yuan, «Physical properties of solid particle thermal energy storage media for concentrating solar power applications,» *Energy Procedia,* vol. 49, nº 1, pp. 1015-1023, 2014.

[30] R. Span y W. Wagner, «A New Equation of State for Carbon Dioxide Covering the Fluid Region form the Triple-Point Temperature to 1100 K at Pressures up to 800 MPa,» *The Journal of Physical Chemistry,* vol. 25, nº 6, pp. 1509-1596, 1996.

[31] V. Vesovic, W. A. Wakeham, G. A. Olchowy, J. V. Sengers, J. T. R. Watson y J. Millat, «The Transport Properties of Carbon Dioxide,» *The Journal of Physical Chemistry,* vol. 19, nº 3, pp. 763-808, 1990.

[32] V. Gnielinski, «New equations for heat and mass transfer in turbulent pipe and channel flow,» *International Chemical Engineering,* vol. 16, pp. 359-368, 1976.

[33] ASME, «Standard for Verification and Validation in Computations Fluid Dynamics and Heat Transfer,» 2009.

[34] C. J. Roy, «Review of code and solution verification procedures for computational simulation,» *Journal of Computational Physics,* vol. 205, pp. 131-156, 2005.

Table caption

Figure caption